



Localised fatigue damage of Carrara marble

G. Royer-Carfagni^a, W. Salvatore^b

^aDipartimento di Ingegneria Civile, Università di Parma, Italy

Email: royer@parmal.eng.unipr.it

^bDipartimento di Ingegneria Strutturale, Università di Pisa, Italy

Email: walter@ing.unipi.it

Abstract

Uniaxial-compression tests at low-cycle fatigue regime were performed on white Carrara marble cylindrical specimens fitted with strain-gauge rosettes. Despite an almost linear elastic response, rock damage is evidenced by a small but progressive and effective translation of the stress-strain graphs, signifying that permanent deformation, rather than appreciable decay in the elastic moduli, is an appropriate correlate of damage. Marked differences have been noticed between the behavior of those specimens with their axis orthogonal to the marble rift plane and those with their axis parallel to this plane. In the first, the most evident sign of failure mechanisms was shear-like deformations, while in the second, it was a marked increase in volume due to microcracking.

1. Introduction

In order to reproduce the degradation process of natural stones, uniaxial compression fatigue tests at low-number-of-cycles were performed on marble quarried from the Altissimo-Mountain near Carrara, yielding a particular quality distinguished by its homogeneity and excellent mechanical characteristics. Cylindrical specimens, 4 cm in diameter and 10 cm high, were tested under varying sequences of two-level programmed loading at a frequency of the order of one cycle per minute. The local material response was measured using rectangular

strain-gauge rosettes placed on the lateral surface of the cylinders approximately at the midpoint along their height, with one gauge parallel to the loading direction. *Ad hoc* control software permitted application of the desired loading schedule through a 200 KN Instron mechanical testing machine and automated recording of the gauge outputs.

Particular attention was dedicated to assessing the possible influences of rock anisotropy. Marble-workers identify three planes in the rock, each at approximately right angles to the others: the rift plane, or *verso*, the grain plane or *secondo* (defining the first and second plane of preferential schistosity, respectively) and the head-grain plane or *contro* (correlated to the surface of the greatest toughness) [1]. The research program included two sample series, compound of cylinders with their bases parallel either to the rift plane (series A1) or to the head-grain plane (series A2). No particular difference in either the ultimate strength or in the elastic moduli could be easily recognized between the A1 and A2 samples, which were classified directly at Carrara using quarrymen's empirical methods.

The specimens were tested using bare steel loading platens. Preliminary investigations had, in fact, shown that interposition of either a lubricant film or any friction-reducing material would cause an undetermined decrease in the confinement of the specimen-ends, which was moreover likely to change randomly with successive loading cycles [2]. The specimen height chosen was 2.5 times the diameter in order to reach a compromise between the effects of platen confinement and those of instability phenomena (i.e. barreling) [3]. To assure the same level of accuracy, all specimens were refaced with a milling machine to obtain variability in planarity of less than 50 μm .

2. Loading orthogonal to the rift plane

A representative response for an A1-type specimen under a monotone uniaxial compression test is reported in Figure 2.1, which shows the average stress σ vs. the local strain recorded by the vertical (ϵ_v), horizontal (ϵ_h) and the 45°-oblique rosette-gauges (ϵ_o), respectively. A slight deviation from linearity is evident only in the final stages of loading, immediately prior to rupture.

Typical diagrams for a cyclically loaded specimen are presented in Figures 2.2a-b-c. Here, the load interval was kept constant nearly throughout the entire test ($\sigma_{\min} = -100$ MPa, $\sigma_{\max} = -4$ MPa), being

increased only from cycle 51 onwards ($\sigma_{\min} = -110$ MPa, $\sigma_{\max} = -4$ MPa) until failure was reached at the 63rd cycle. Some aspects, peculiar to the general fatigue-behavior of marble, are evidenced by the diagrams. In general, both ϵ_v (Figure 2.2a) and ϵ_h (Figure 2.2b) present a slightly non-linear dependence on σ only in the very first loading step - the material response remains almost linear from the second cycle onwards with no significant change in slope. A small but effective translation of the

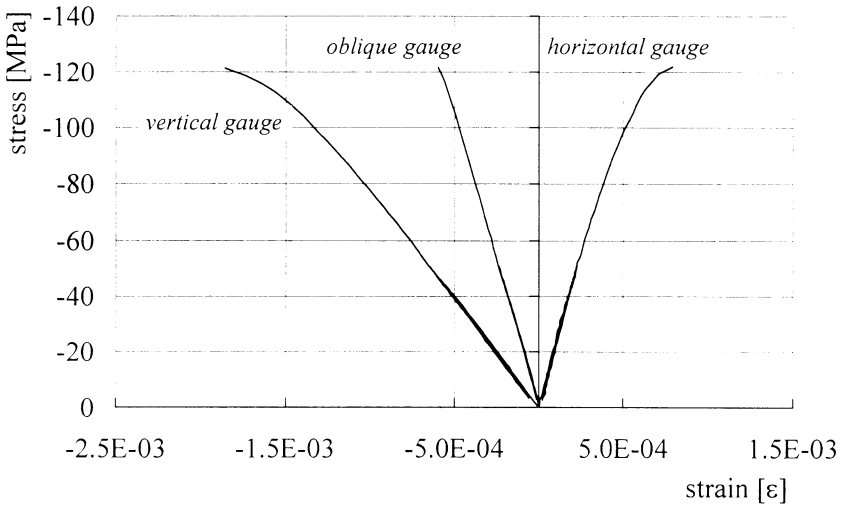


Figure 2.1: Typical σ - ϵ relations for a static compression test (test AM-A1-n11): a) vertical gauge, ϵ_v ; b) horizontal gauge ϵ_h ; c) 45°-oblique gauge ϵ_o .

diagrams is however recognizable, denoting that repetitive load cycles produce progressive permanent deformation for both ϵ_v and ϵ_h , rather than substantial decay in the elastic moduli. Strain accumulation was recorded for ϵ_o , as well (figure 2.2c), but this was comparatively much less than for ϵ_v and ϵ_h . In the first period of the loading schedule ($\sigma_{\min} = -100$ MPa, $\sigma_{\max} = -4$ MPa), the permanent deformation tends towards a limit value, and the σ - ϵ graphs overlap on a limit hysteresis loop. When the load interval is increased, the permanent strains again start to accumulate, until failure is reached (last cycles in Figures 2.2).

Such behavior can be better understood through the diagrams in Figures 2.3, which report as a function of n , the maximum and minimum values reached in the n^{th} cycle by ϵ_v , ϵ_h and ϵ_o , respectively. In Figure 2.4

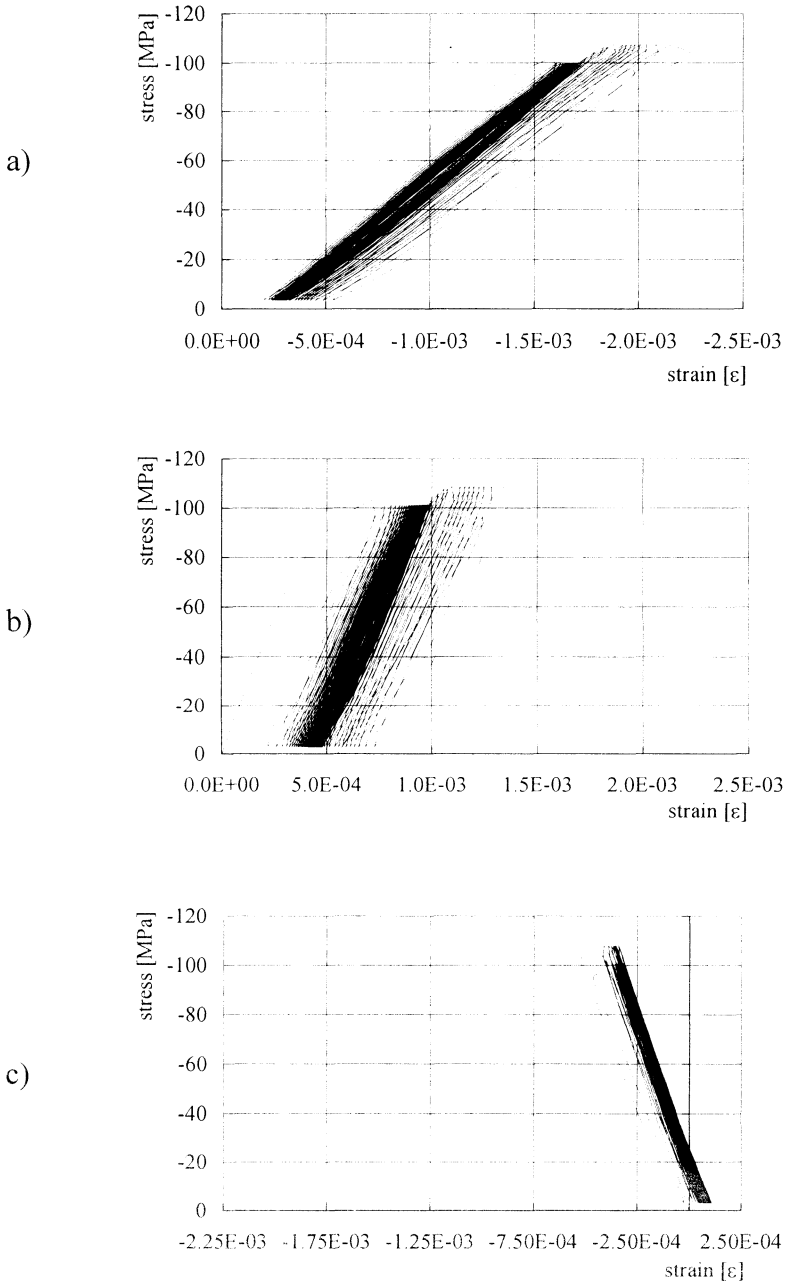


Figure 2.2: Typical σ - ϵ relations for cyclic compression test (test AM-A1-n5):
a) vertical gauge, ϵ_v ; b) horizontal gauge ϵ_h ; c) 45°-oblique gauge ϵ_o .

we report instead, still as a function of n , the quantities Δ_{\max} , Δ_{\min} , ϵ_{\max}^s , ϵ_{\min}^s , defined as

$$\Delta_{\max} = \Delta_{\max}(n) = \max_{n\text{-cycle}} \left[\frac{\epsilon_1 + \epsilon_1}{2} \right], \quad \Delta_{\min} = \Delta_{\min}(n) = \min_{n\text{-cycle}} \left[\frac{\epsilon_1 + \epsilon_1}{2} \right], \quad (1)$$

$$\epsilon_{\max}^s = \epsilon_{\max}^s(n) = \max_{n\text{-cycle}} \frac{\epsilon_1 - \epsilon_2}{2}, \quad \epsilon_{\min}^s = \epsilon_{\min}^s(n) = \min_{n\text{-cycle}} \frac{\epsilon_1 - \epsilon_2}{2}, \quad (2)$$

where ϵ_1 , ϵ_2 are the principal strains calculated from the gauge-rosette outputs, and the maximum and minimum are intended in the n^{th} cycle. It is clear that the surface-dilatations Δ_{\max} , Δ_{\min} are correlated with volume increases, while ϵ_{\max}^s , ϵ_{\min}^s are the shearing strains ([3], Art.16). The opening of cracks is clearly revealed by a permanent increase in Δ , while no volume increase occurs wherever shear slip bands alone develop.

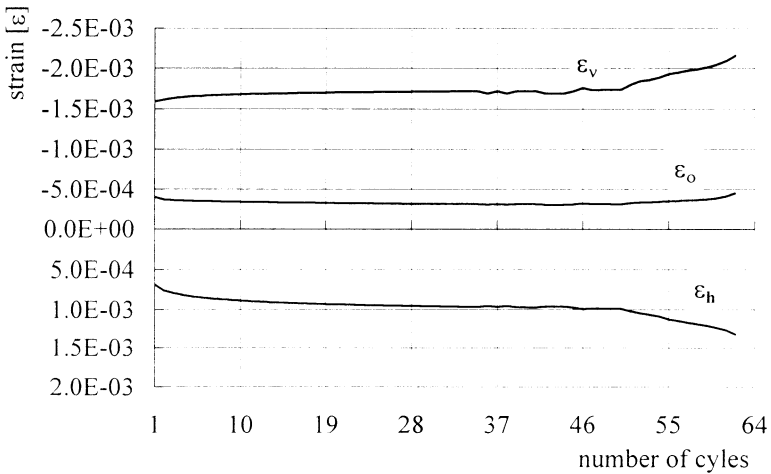


Figure 2.3: Maximum and minimum values of a) ϵ_v , b) ϵ_h , c) ϵ_o , as a function of the number of cycles.

The very first period (cycles 1 to ~5-6) corresponds to the initial, fast, degradation phase, where a rapid increase in volume is accompanied by a permanent increase in shear deformation. A second period follows, characterized by pseudo-linear dependence on n of all the components, ϵ_v , ϵ_h and ϵ_o , and consequently of Δ_{\max} , Δ_{\min} , ϵ_{\max}^s , ϵ_{\min}^s . The final phase, beginning when the load interval is increased ($n=51$), corresponds to the mechanism leading to failure. At this stage the increase in dilatation is negligible with respect to the increments in shearing strain.

signifying that the material tends to deform with a shear-like mechanism.

Throughout the test, the principle directions of strain remained approximately those of the vertical and horizontal gauge. This is evident from the graphs of Figure 2.5 that show, once again as a function of n , the two extreme values θ_{\min} and θ_{\max} reached by angle θ in each load cycle, that identify the principal strain directions with respect to the two perpendicular rosette-gauges. What should be noted is that when the load is increased (starting with cycle 51), angle θ_{\min} and, even more so, angle θ_{\max} also tend to increase, up to 0.20 rad ($\approx 11^\circ$).

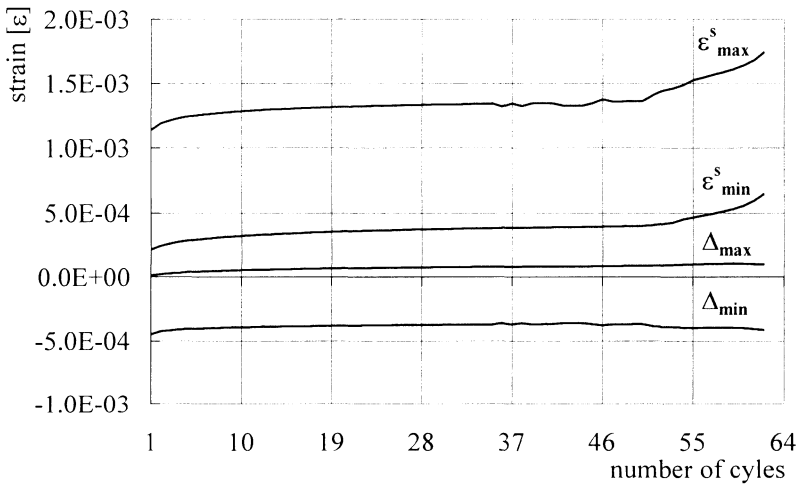


Figure 2.4: Values of Δ_{\max} , Δ_{\min} , ϵ^s_{\max} , ϵ^s_{\min} vs. the number of cycles.

If the number of cycles, n is reported on a logarithmic scale, the graphs of Δ_{\max} , Δ_{\min} , ϵ^s_{\max} , ϵ^s_{\min} in Figure 2.4 assume the shapes illustrated in Figure 2.6. These are characterized by a linear first branch, which in this case begins at cycle $n=1$ and continues up to $n=51$. Since the permanent deformation, even in the very earliest cycles, is very well approximated by a linear function of the logarithm of n , it is natural to correlate this linear branch of the graphs with a steady-state evolution of the damage. The final process leading to failure ($n=51$ onwards) does not follow this steady relationship, as evidenced by the last branches of the graphs. Here the shear strains show a marked increase, while the dilatations maintain the same steady trend as in the very first cycles. This is evidence that microcracking follows the same uniform progression even in the final cycles, while shear deformations experience a sudden increase which eventually culminate in rupture.

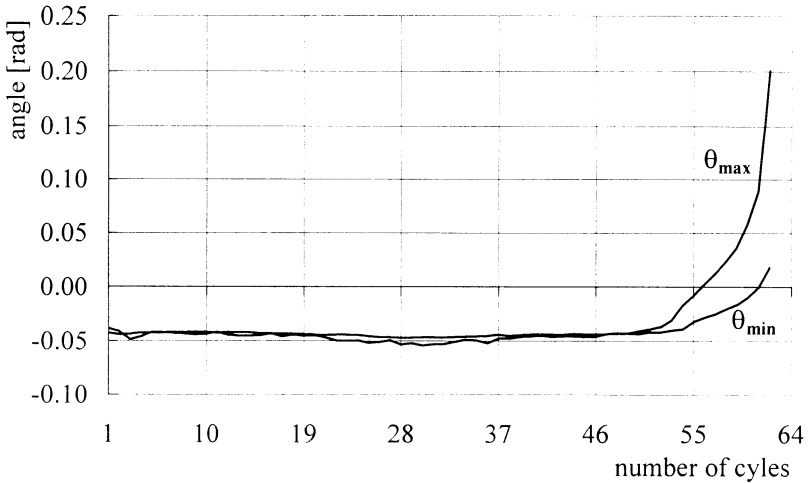


Figure 2.5: Values of θ_{\min} and θ_{\max} , as a function of the number of cycles.

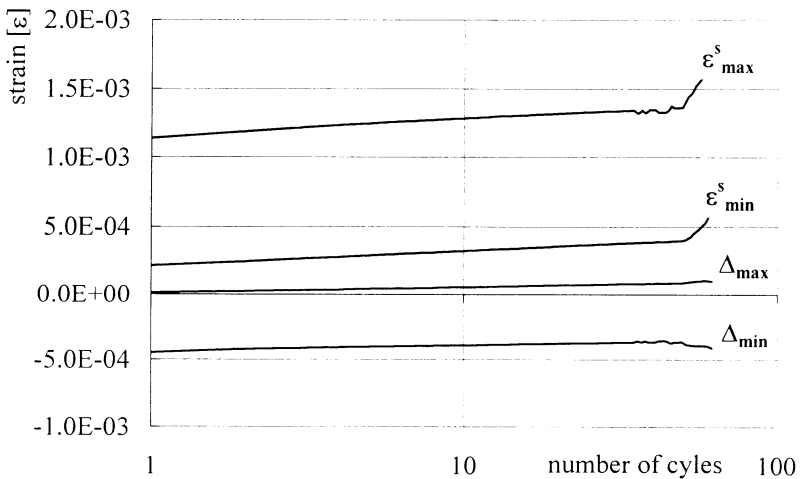


Figure 2.6: Values of Δ_{\max} , Δ_{\min} , ϵ_{\max}^s , ϵ_{\min}^s vs. n -logarithmic scale.

3. Loading orthogonal to the head-grain plane

In this second series of tests on type A2 samples, the plane of preferential schistosity is now parallel to the loading direction. Intuitively, one would expect pseudo-vertical cracks to begin to open; this is confirmed by comparing the diagrams of Figure 2.1 to those reported in Figure 3.1,

again corresponding to typical results for static compression testing.

Figures 3.2 a-b-c are representative of the material response to cyclic loading (and report, analogously to Figure 2.2, the average stress as a function of local strains ε_v , ε_h and ε_o , respectively). This time the load interval was kept constant from the 1st to the 165th cycle (from $\sigma_{\min} = -95$ MPa to $\sigma_{\max} = -4$ MPa), until equilibrium on a limit hysteresis loop was reached. Afterwards, the minimum stress level was gradually decreased, down to $\sigma_{\min} = -110$ MPa, until failure of the specimen at the 185th cycle. These diagrams are qualitatively similar to those of Figure 2.2, but differ in two features: the horizontal gauge reports a much greater deformation than in the previous case, especially in the last cycles, and secondly, the oblique gauge experienced a positive strain in the final cycles.

The peculiarities of type-A2 specimens are more evident in the diagrams of Figures 3.3 and 3.4, which give, as in Figures 2.3 and 2.4, the maximum and minimum values reached in the n^{th} cycle by ε_v , ε_h , ε_o and Δ_{\max} , Δ_{\min} , ε_{\max}^s , ε_{\min}^s , respectively. Like type-A1 specimens, the initial phase (cycles 1 to ~ 15) is characterized by a rapid increase in both dilatation and shearing strain, followed by a second stage (up to $n \cong 165$) in which the strains evolve almost linearly with n . These two phases correspond to the steady-state development of permanent deformation. Figure 3.5, which uses a logarithmic scale for n , evidences once again the uniform evolution of the phenomenon and the very good approximation afforded by the straight branches.

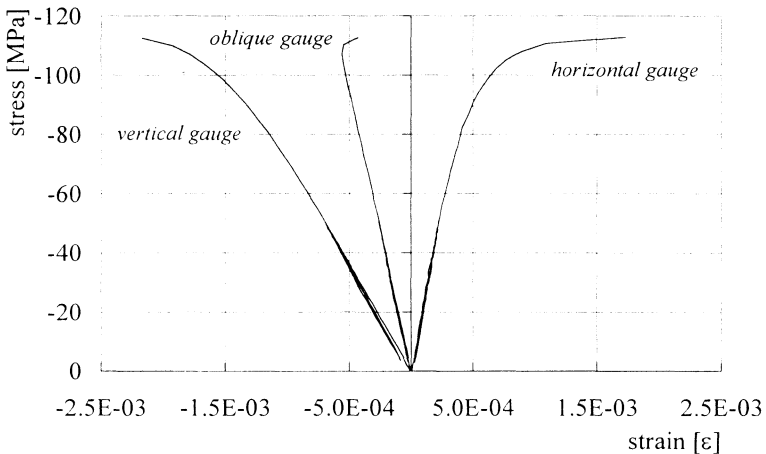


Figure 3.1: Typical σ - ε relations for a static compression test for A2 specimens (test AM-A2-n4): a) vertical gauge, ε_v ; b) horizontal gauge ε_h ; c) 45°-oblique gauge ε_o .

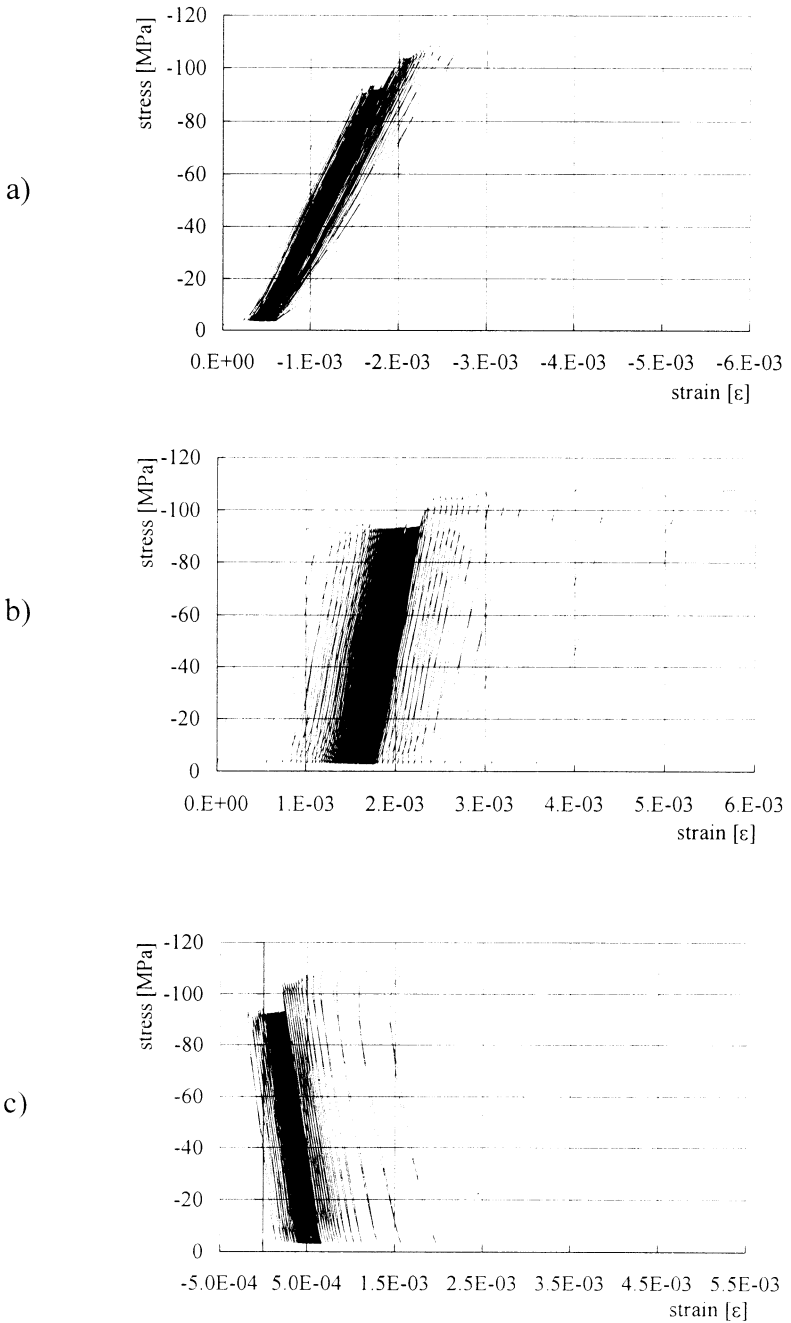


Figure 3.2: σ - ϵ relations for cyclic compression test on A2 specimens (test AM-A2-n2): a) vertical gauge, ϵ_v ; b) horizontal gauge ϵ_h ; c) 45°-oblique gauge ϵ_o .

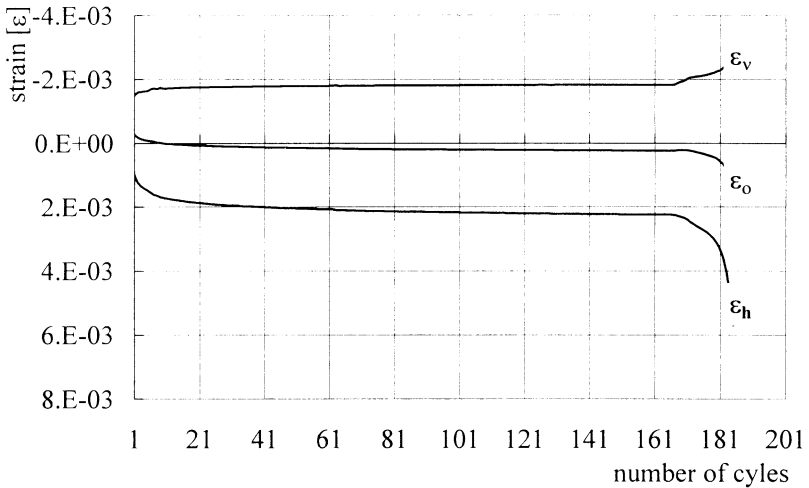


Figure 3.3: Maximum and minimum values of a) ϵ_v , b) ϵ_h , c) ϵ_o , as a function of the number of cycles for type A2 specimens.

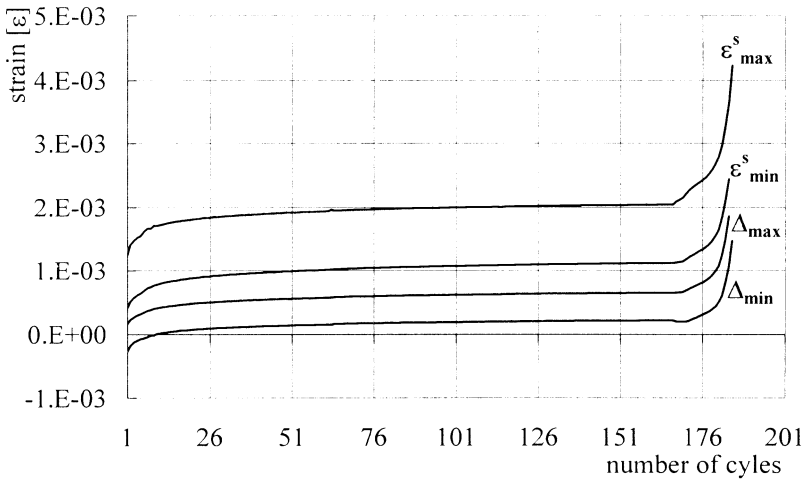


Figure 3.4: Values of Δ_{\max} , Δ_{\min} , ϵ_{\max}^s , ϵ_{\min}^s vs. n for type A2 specimens.

Marked differences between A1 and A2 specimens are instead present in the final phases, from $n=165$ onwards. Very strong increments in shear strain are still evident (Figures 3.4 and 3.5), but these are accompanied by increases in dilatation that are much more marked than previously (Figures 2.4, 2.6). By examining the graphs in Figure 3.3, it can be seen that in the last cycles ϵ_h results to be much greater than ϵ_v , suggesting that

a fundamental role in the mechanism leading to failure is this time played by the opening of pseudo-vertical microcracks.

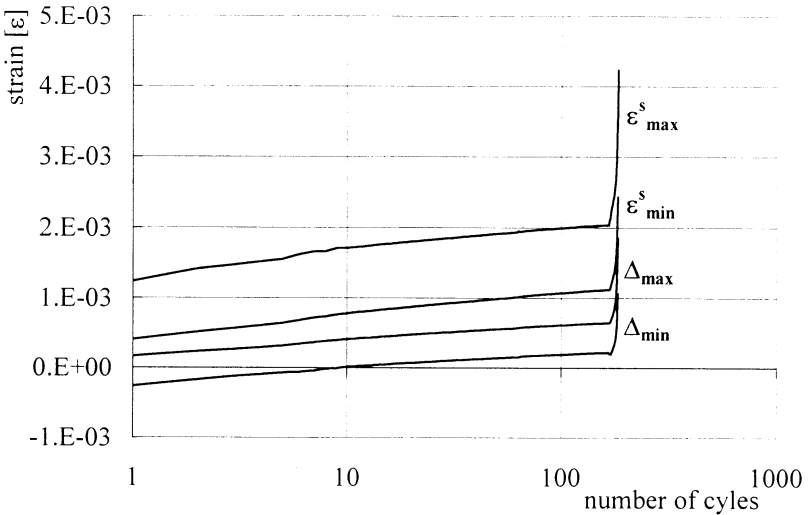


Figure 3.5: Values of Δ_{\max} , Δ_{\min} , ε_{\max}^s , ε_{\min}^s vs. $\log n$, for type A2 specimens.

4. Concluding remarks

In spite of the highly “local” character of our observations, relying on the outputs of strain-gauge rosettes alone, some concluding remarks may be useful to foster further, more sophisticated, experimental research.

It is our opinion that the proper choice for the material internal variable best able to quantify cumulative damage is the accretion of permanent deformation, rather than significant decay in the elastic moduli. In all our experimental trials [2] we have observed an initial steady trend during which, maintaining the extreme stress intervals fixed, non-recoverable strains grow *linearly with the logarithm of the number of cycles*. In this initial period, both dilatations and shear strains accumulate, with a small prevalence of shear with respect to dilatation in those specimens loaded at right angles to the rift plane.

Marked peculiarities induced by rock anisotropy are instead present in the final stages leading to failure. We have strong evidence that essentially shear-like deformation, probably due the development of slip bands at 45° to the loading direction, is the leading failure mechanism for those specimens loaded orthogonally to the direction of major



schistosity. Microcracking is instead more likely to play an important role when the specimen is loaded parallel to this plane.

Acknowledgments

We wish to thank Mr. F. Pratelli, Mr. L. Pagni and Mr. M. Di Ruscio for their skillful assistance in performing the experiments. Partial support of the European Community under Contract SMT4-CT96-2130 is gratefully acknowledged.

References

- [1] Dolci, E., *Carrara Cave Antiche*, Comune di Carrara, Tipolito Mario Pezzini, Viareggio, 1980.
- [2] Sanpaolesi, L., Royer-Carfagni, G., Salvatore, W. & Valvo, P., Fatigue tests on Natural Building Stones, 1st year report of the EC Research Program SMT4-CT96-2130 *Characterization of Natural Properties and Damage of Natural Building Stones in Historical Monuments*, 1998.
- [3] Biot, M.A., *Mechanics of Incremental Deformations*, John Wiley & Sons, New York, 1965.
- [4] Love, A.E.H., *A Treatise on the Mathematical Theory of Elasticity*, Dover Publications, New York, 1944.